

RSC Advances



This is an *Accepted Manuscript*, which has been through the Royal Society of Chemistry peer review process and has been accepted for publication.

Accepted Manuscripts are published online shortly after acceptance, before technical editing, formatting and proof reading. Using this free service, authors can make their results available to the community, in citable form, before we publish the edited article. This *Accepted Manuscript* will be replaced by the edited, formatted and paginated article as soon as this is available.

You can find more information about *Accepted Manuscripts* in the [Information for Authors](#).

Please note that technical editing may introduce minor changes to the text and/or graphics, which may alter content. The journal's standard [Terms & Conditions](#) and the [Ethical guidelines](#) still apply. In no event shall the Royal Society of Chemistry be held responsible for any errors or omissions in this *Accepted Manuscript* or any consequences arising from the use of any information it contains.



Journal Name

ARTICLE

Different ordering carbonaceous structures synthesized by bubbled Ar or He plasmas inside methylene blue solutions with contrasting *Escherichia coli* growth inhibition effects

Received 00th January 20xx,
Accepted 00th January 20xx

DOI: 10.1039/x0xx00000x

www.rsc.org/

D. Zaharie-Butucel,^a J. Papp^a, C. Leordean^b, S. D. Anghel^a

This work is a comparative study on the synthesis of carbonaceous structures with different ordering, aided by a atmospheric pressure plasma in contact with methylene blue aqueous solutions, by utilizing two different inert plasma gases, argon and helium respectively. The study follows the diagnosis of the two plasmas by Optical Emission Spectroscopy, their different degradation effects on methylene blue solutions and the characterization of the carbonaceous structures obtained as a result of plasma treatment with Transmission Electron Microscopy, Raman and X-ray Photoelectron Spectroscopy. The carbon based structures obtained with the helium plasma have a higher degree of ordering and are larger in size compared to the Ar plasma ones. The bacterial growth inhibition assays show opposite behaviours: one structure inhibits the growth while the other favours it.

Introduction

Carbon based nanoparticles are materials composed for the most part of carbon with one or more dimensions less than 100 nm. They include fullerene, carbon nanotubes (CNT), the graphene family, carbon dots, nanodiamonds, nanofoam, nanohorns and nano-onions. This class of nanoparticles has unique physiochemical properties (light weight, high tensile strength, thermal/chemical stability, conductivity) which make them suitable in many fields including biomedical applications such as tissue scaffolds, gene drug-delivery vehicles, anti-tumor agents, fluorescent contrast agents^{1–3}.

There is a large variety of synthesis methods such as: arc discharge, laser ablation, chemical vapour deposition (CVD), electrolysis and chemical methods. Most of these techniques are highly complex in their reactor design. The physical methods arc discharge and laser ablation are energy extensive methods and they require solid carbon/graphite as targets. It is difficult to control the process hence the need to refine the products. CVD has the advantage of using an easily available hydrocarbon gas as precursor however it requires high temperatures. Electrolysis requires graphite cathodes and high temperatures⁴. The majority if not all of the chemical synthesis methods are time consuming and utilize dangerous reagents that provide the necessary energy to modify the

structure of the carbon precursors into the desired one.

Several of the carbon nanoparticles are easily produced however such as carbon dots. They can be made by simple burning or microwave heating of organic matter and even from waste natural products⁵. The obtained particles may have at the surface hydroxyls, carbonyl, carboxyl groups and amine groups which facilitates their functionalization.

In the last years plasma in contact with liquids has become a highlight in the area of plasma mostly due to their great biomedical and environmental potential applications as they are produced in ambient conditions at atmospheric pressure. This aspect is visible in the large variety of experimental set-up's. However their ignition mechanisms are not yet elucidated completely.

The discharges in contact with liquids are known to generate oxidative species, flux of charged or heavy particles, UV irradiation, shock waves, thermal effects⁶.

These types of plasma are non-thermal (the electron temperature is different from the ion temperature) in nature leading to numerous chemical reactions based on electron collisions. As a result of these reactions strong oxidative species are produced such as hydroxyl, atomic oxygen, hydrogen peroxide or ozone and even some metastable species are formed: singlet oxygen and superoxide.

All these characteristics suggest that plasma in liquids is suitable for sterilization, microorganism inactivation, nanoparticle synthesis and functionalization and dye degradation. Recently, gold nanoparticles were synthesized assisted by plasma in aqueous solutions and it was proved to be a faster and more efficient synthesis method compared to the standard chemical ones^{7,8}. Another research group successfully utilized a plasma in organic solution as a

^a Babes-Bolyai University, Mihail Kogalniceanu 1, Cluj-Napoca, Romania, 400084

^b Interdisciplinary Research Institute in Bio-Nano-Sciences, Treboniu Laurian 42, Cluj Napoca, Romania, 400271

† Footnotes relating to the title and/or authors should appear here.

Electronic Supplementary Information (ESI) available: [details of any supplementary information available should be included here]. See DOI: 10.1039/x0xx00000x

simultaneous reduction and functionalization method for graphene oxide⁹.

In this context we previously reported for the first time, the capacity of Ar bubbled plasma generated in a water based solution to degrade a cationic dye, methylene blue (MB) and simultaneously aid in the synthesis carbon based nanoparticles¹⁰. The dye degradation capacity of plasma discharges in contact with aqueous solutions and specifically with MB, was studied by others before. The general approach was to use highly oxidizing gases such as oxygen and ozone and to optimize the system energetically since there was an eager interest in obtaining high degradation yields for the plasma discharge. This approach proved to be effective in dye degradation applications. By utilizing inert gases such as argon or helium we show that the plasma could have a double role: on the one hand it decomposes the dye molecules however not fully so that on the other hand it could assist in the synthesis carbon based nanoparticles and microparticles. Furthermore, in this work we focus on the influence of the plasma gas on the particle structure and morphology, we do a more in depth particle characterization and show that the obtained carbonaceous structures have a different bacterial growth inhibition effect as well one inhibits the growth while the other favours it.

Experimental

Methodology and apparatus

The procedure for the nanoparticle synthesis is rather simple: a solution of MB (25 ml, 100 mg l⁻¹), undergoes plasma treatment for a time frame of solely tens of minutes. The plasma discharge, generated inside bubbles in the dye solution, has a degradation effect and concurrently carbon structures are formed. No additional reagents are used. For this study two plasma gases were used namely argon (Ar) and helium (He) at extremely low flow rates (0.35 l min⁻¹). The different degradation process and carbon structures synthesis were investigated.

The plasma reactor used is described in more detail elsewhere¹⁰. Briefly, it consists of a metallic wire electrode placed via a holder piece in a quartz tube through which plasma gas (Ar or He) flows with a flow rate of 0.35 l min⁻¹. The electrode is made of kanthal A-1 and its upper end being powered with high sinusoidal voltage (1.7 kV, 10.2 MHz) generated with a laboratory made free-running oscillator¹¹. The glass tube is vertically immersed in the liquid at a depth of 15-20 mm and the plasma is generated inside bubble gas between the powered electrode and the bubble wall. The mean plasma power was estimated to be of about 16.5 W. A schematic representation of the synthesis procedure is presented in figure 1.

The bacterial growth inhibition capacity of the carbon particles was assessed by UV-VIS spectroscopy measuring the optical density of the bacterial suspensions at 620 nm. Different volumes (10 µl, 30 µl, 50 µl, 80 µl and 100 µl) of particles were incubated with nutrient broth and *E.coli* suspension for 24

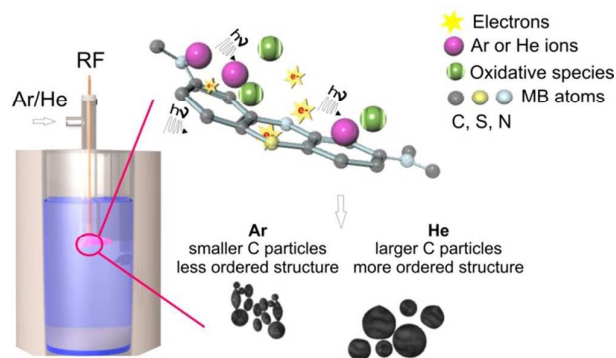


Figure 1 - Schematic representation of the synthesis procedure and mechanism.

hours. The control experiment was made in the same manner except using equal volumes of distilled water instead of the particles. The contribution of the nutrient broth to the absorption spectra was removed by doing a background with the same dilution in each case only for the broth.

Characterization techniques

The bubbled plasma was diagnosed via Optical Emission Spectroscopy (OES) by analyzing the emission spectra in distilled water for the two plasma gases Ar and He. The optical emission was collected with a HR4000CG-UV-NIR Ocean Optics High-Resolution Fiber Optical Spectrometer with the wavelength range of 254 – 965 nm controlled with the SpectraSuite software. The plots are the result of average of 11 scans (500 ms integration time) in order to compensate the light fluctuation during an ignition-extinction discharge cycle. To identify the atomic lines and the molecular bands in the emissions spectrum we used a dedicated software Spectrum Analyzer version 1.7. The atomic excitation temperature of Ar was calculated from the ratio between the relative intensities of the lines at 840.82 nm and 842.47 nm and the atomic excitation of He was calculated from the relative intensities of the lines at 728.14, 706.52, 667.82, 587.56 and 501.57 nm by using the Boltzmann plot method. The temperature of excitation of rotational states of the OH[•] radicals, $T_{rotOH^{\bullet}}$ was estimated by finding the best fit (chi-square method) of the measured molecular spectra with the synthetic spectra generated by the LIFBASE simulation software¹². The Stark broadening of the hydrogen α line was used to determine electron densities based on the next formula: $\Delta\lambda_S = 1.78 \cdot (n_e/10^{17} \text{ cm}^{-3})^{2/3}$. The H α line in the emission spectrum was fitted with a Voigt profile and then the FWHM of the Voigt profile was corrected with the instrumental, Doppler and van der Waals broadenings to obtain the Stark broadening.

To evaluate the plasma degradation effect Molecular Absorption Spectroscopy was used and a Jasco V-630 UV-vis spectrophotometer was employed. Aliquots of the MB solution were collected after different plasma treatments times and the absorption spectra were recorded in quartz cuvettes with

an optical distance of 1 cm, 20 minutes after the plasma treatment ended.

Transmission Electron Microscopy (TEM) was used to characterize the morphology of the particles. The images were obtained with a Tecnai F20 field emission, high resolution Transmission Electron Microscope operating at an accelerating voltage of 200 kV and equipped with Eagle 4k CCD camera.

Raman measurements were performed with a Witec Alpha 300 R confocal Raman microscope, using a 532 nm Nd-Yag laser excitation line, directed through a 100X microscope objective. The samples were drop-cast on Si/SiO₂ substrates and air dried. The spectra deconvolution was made with a combination of Lorentz and Breit-Wigner-Fano (BFW) lines suitable for carbon structures¹⁴.

To investigate the structure of the particles at the surface, X-ray Photoelectron Spectroscopy (XPS) measurements were performed using a SPECS PHOIBOS 150 MCD system, equipped with a monochromatic Al K_α X-ray source (250 W, $h\nu = 1486.6$ eV). The pressure in the analysis chamber during the measurements was around 10⁻⁹ mbar. The binding energy scale used as reference was the C 1s peak at 285 eV and the high resolution spectra were measured using 0.05 eV step size. The measured sample was prepared by placing several droplets of the solution on a glass plate. It was left drying in a closed space which led to the formation of a thin layer. The elemental concentrations at the surface were estimated by integrating the peaks assuming a Shirley background in the CasaXPS software.

Results and discussions

Active species in the plasma

The emission of the plasma is relevant in identifying the active species present in the discharge and in this case the emission in the UV-NIR range is important. Apart from the emission lines coming from the plasma gas, Ar and He respectively for the two plasmas, the emission lines of hydrogen (H_α) and oxygen are present in the spectra. The He plasma emission spectrum in water is presented in figure 2. One difference comes from the first negative system of N₂⁺ (391.44 nm) which is absent in the Ar plasma emission. The N₂⁺ emission is attributed to Penning ionization with helium metastable species^{15,16} present in the He plasma, whose excitation energy (23.07 eV) is comparable to that of the ionic molecule N₂⁺ (18.8 eV). One important species, due to its highly oxidative character which aids in the dye degradation process, is the OH[•] radical. This radical is present in the discharge as a result of water molecules dissociation and it has an emission band in the UV region with the band head at 308.9 nm. The plasma characteristics determined from the emission spectra are presented in table 1.

While the electron densities number is of the same order 10¹⁵ cm⁻³, the atomic excitation temperature of Ar is more than two times larger than the He excitation temperature. These values are similar to values reported by others for plasma discharges when one or both of the electrodes are liquid⁶. One important

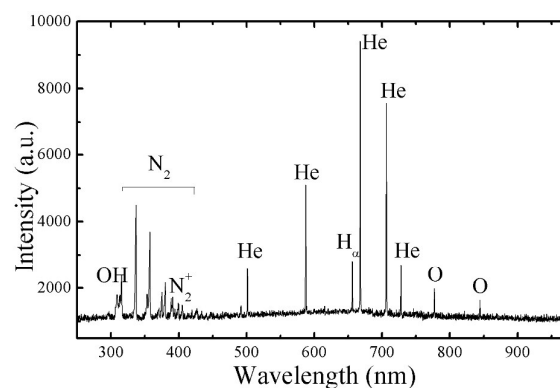


Figure 2 - Emission spectrum of plasma generated in He bubbled in water.

result is that the OH[•] emission band head of the Ar plasma is approximately four times higher than for the He plasma which might indicate that there is a greater quantity of hydroxyl radical generated in the Ar plasma as the emission is linked to the ground state density of the species. According to Bruggeman *et al* in plasma physics three types of processes are responsible for OH[•] production: electron, metastable induced or thermal dissociation of water molecules¹⁷. Thermal dissociation and metastable induced dissociation are suspected to induce this difference since electron densities are of the same order of magnitude. Thermal dissociation of water is most efficient around 3300 K¹⁷ that is why this process is expected to have a greater contribution at the OH[•] density in the case of Ar plasma which has higher temperatures in the discharge volume compared to the He plasma.

Metastable induced water dissociation is a less probable process in the case of He plasma because He_m are involved in Penning ionization with N₂ molecules as stated previously which results in a lower OH[•] density.

Spectroscopic study of MB during plasma degradation process

There are three main mechanisms for dye degradation in plasma in liquids: electron bombardment, ion collision and radical induced degradation. The two plasmas investigated have a different degradation effect on the MB solution, easily evaluated by UV-vis spectroscopy. Figure 3 depicts the UV-vis absorption spectra of the MB solutions after different plasma time treatments which present the specific band at 663 nm ($n-\pi^*$) and a shoulder at 613 nm. After 40 minutes for the Ar plasma and 60 minutes for the He plasma, the main absorption band (663 nm) disappears and becomes a flat line suggesting that the MB solution was completely discolored. Electron induced degradation is a process that appears for both plasmas.

Table 1- Plasma gas atomic excitation temperatures, OH[•] rotational temperature and electron densities number for the Ar and He plasmas

	T _{exc plasma gas atoms} (K)	T _{rotOH} (K)	n _e (cm ⁻³)
Ar plasma ¹⁰	6080	1990 ± 10 %	3.79·10 ¹⁵
He plasma	2555	960 ± 15 %	3.46·10 ¹⁵

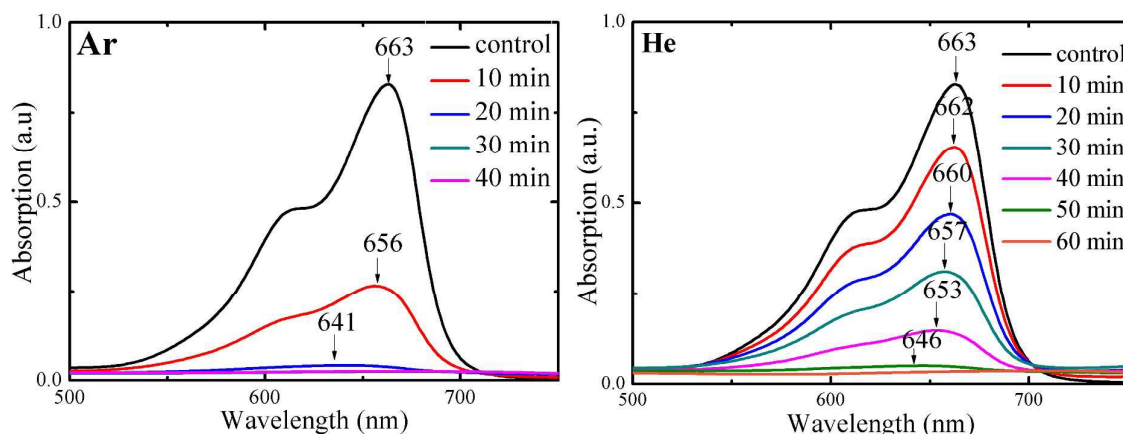


Figure 3 - The evolution of the main absorption band with the increase of the time treatment for the Ar and He plasmas

The difference could be explained by the hydroxyl radical density estimated from the emission measurements, which was said to be higher in the case of the Ar plasma. In addition to that, a gradual blue shift of the main band appears which is consistent with a N-demethylation of the MB molecule in a step-wise manner (i.e. methyl groups are removed one-by-one)^{10,18,19} an effect induced by the action of the plasma on the MB molecules. As suggested by the UV-vis absorption spectra, the degradation process is greatly influenced by the working gas. In the case of He plasma the degradation process seems to be linear as reflected by figure 4 while in the case of Ar plasma tends to be an exponential process. The concentration drop for the Ar plasma is the greatest in the first 20 minutes of treatment compared to the He plasma for which the concentration decreases linearly for the complete degradation process. This fact suggests that there is a degradation mechanism in the Ar plasma which does not occur in the He plasma. The most logical assumption is that the mechanism is related to the type of gas used. The argon metastable states Ar_m^* (3P_2 , 3P_0) are already said to produce hydroxyl in water discharges which adds to the degradation^{20,21}. Ar_m^* can directly decompose MB as well²⁰. The helium atoms excited on metastable states He_m (3S_1 , 1S_0) are also cap-

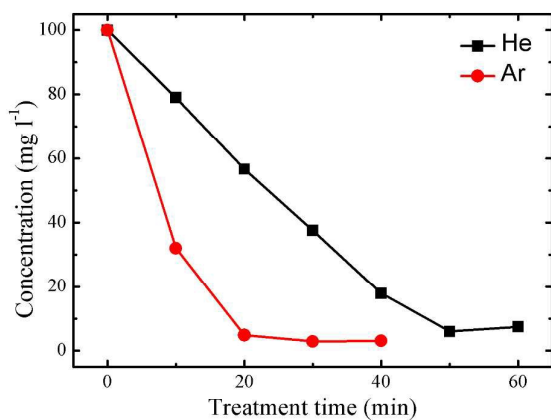


Figure 4 - The evolution of the MB concentration with plasma time treatment as parameter for the Ar and He plasmas.

able of water dissociation to produce hydroxyl¹⁷ therefore the direct decomposition of MB by Ar_m^* is the process which might explain the increased degradation of MB with Ar plasma. This process is probably correlated to the greater atomic mass of Ar compared to He. An ion with a greater atomic mass would gain energy in the rf electric field, would transfer the energy by means of collisions more efficiently than a smaller atomic mass ion, break the molecular bonds and lead to a more aggressive degradation process.

Morphological characterization

As our aim was to provide a characterization of the particles and at the same time to elucidate the synthesis process, we recorded TEM images of the solutions at the maximum treatment time and an intermediate time (20 minutes) for both the Ar and He plasmas. These images are presented in figure 5.

The TEM images for the Ar plasma intermediate time reveal the presence of particle aggregates of different morphologies. The plasma has a destructive effect on the particles as the time treatment increases leading to the formation of a web-like structure (figure 5 left C, D). The particles seem to be a part of this structure suggesting that the web is most likely the residue from the degradation of the particles by the plasma. One might argue that the residue actually consists of the primary dye degradation products however if that were the case, the web is expected to appear even in the intermediate time images not just in the ones at the end of treatment.

As in the case of the Ar plasma, the TEM images of the particle obtained for the He plasma intermediate time reveal that the obtained particles are polydisperse and present mainly spherical shapes, see figure 5 (right A,B). There are also sheet-like structures presenting as a uniform thin layer. In some areas the particle are stacked together with the sheet-like structures and in others the particles seem to be detaching from the sheets. This could be one of the stages of the formation of the particles. As the time treatment increases the particles themselves are affected by the plasma and not just the precursor. In this case, our assumption is that the particles are broken by the plasma because the remaining particles tend to be only irregular in shape. At the same time the sheet-like

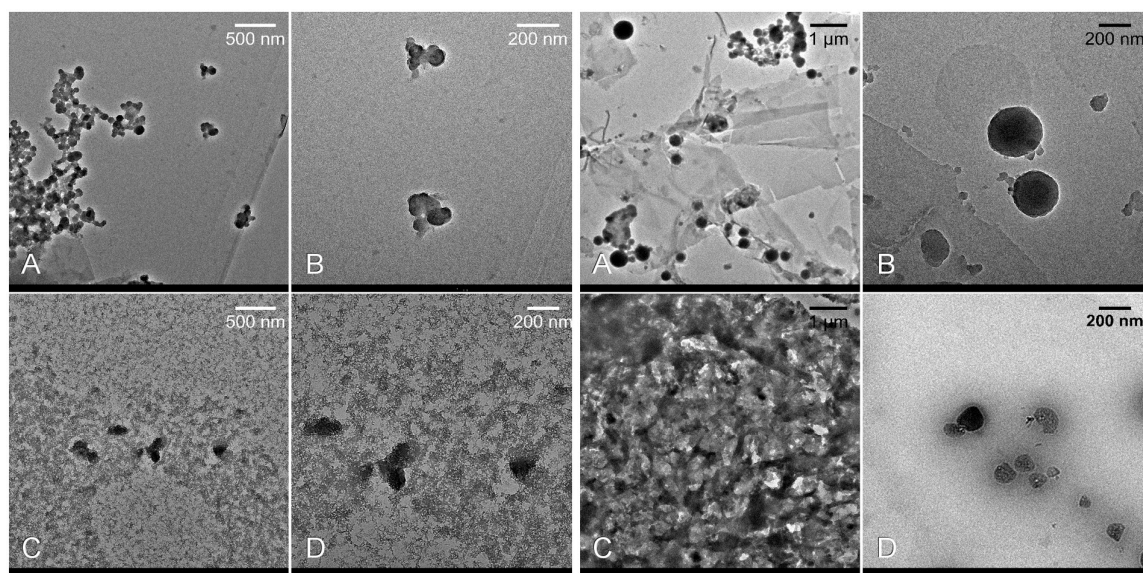


Figure 5 - TEM images of the Ar plasma carbon structures (left) obtained at different time treatments: A,B-20 minutes C,D- 40 minutes and of the He plasma carbon structures (right) obtained at different time treatments: A,B-20 minutes C,D- 60 minutes.

structures are no longer uniform in thickness suggesting that the plasma degrades the structure and simultaneously residue coming from the particles and the MB degradation products build-up to form a new structure.

Compared to the previous case in which a web of residue is developed during plasma treatment, the sheet-like structure is essentially different as it extends over broad areas. An important particle analysis is the size distribution presented in figure 6. The histograms were built using the intermediate time TEM images making over 200 counts in the ImageJ software. The mean particle size is different in the two cases: 79 nm for Ar and 260 nm for He. The explanation lies in the different degradation process. UV-vis analysis revealed the fact that the Ar plasma is more aggressive in terms of degradation and thus faster allowing less time to the formation of the of

monodispersity in size from the standard deviation (SD). The Ar plasma leads to the formation of more monodisperse particles compared to the He plasma. This fact can also be explained by the slower degradation process in the case of He plasma which enables the formation in great proportion even of bigger particles.

Based on the TEM images we assume that there are two simultaneous processes: the formation of the particles from the MB molecules and the degradation of the particles by the plasma which produces a varied morphology and dimensions for the particles. The Ar plasma to nanoparticles with lower polydispersity and the He plasma leads to the formation of microparticles with increased polydispersity. It is also important to note that even though the plasma provides the building blocks for the particles formation it is also involved in

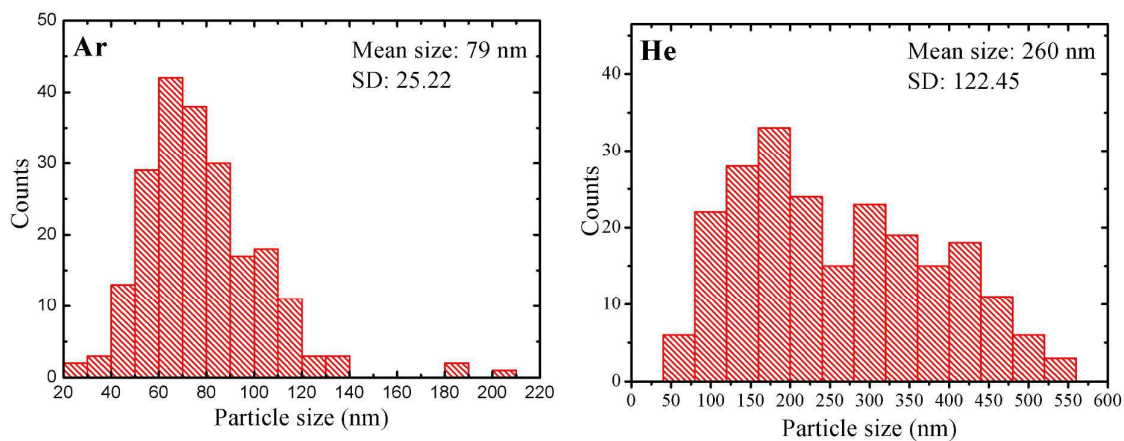


Figure 6 - Particle size distribution for the particles obtained with Ar plasma(left) and for the He plasma respectively (right)

their degradation process therefore there is a compromise to be made between reaching complete degradation and avoiding particle degradation.

Raman spectroscopy

The Raman spectra of the solutions obtained after the maximum treatment time and an intermediate time for the Ar and He plasma are presented below in figure 7 and the Raman deconvolution peaks characteristics are depicted in table 2. Ferrari *et al* describe the amorphization trajectory of carbon structures from sp^2 graphite to tetrahedral sp^3 carbon diamond and their respective Raman spectra characteristics¹⁴. Along the trajectory three main stages are identified: stage 1 graphite-nanocrystalline graphite, stage 2 nanocrystalline graphite- low sp^3 amorphous carbon and stage 3 a-C – tetrahedral amorphous carbon. Graphite comprises of layers of sp^2 carbon atoms arranged in a honeycomb structure placed one on top of the other. The Raman spectrum of graphite is characterized by two main features termed the G and D peaks. The G peak, found in the 1580–1600 cm^{-1} area and the D peak, around 1350 cm^{-1} , are usually assigned to zone center phonons of E_{2g} symmetry and K-point phonons of A_{1g} symmetry, respectively^{14,22}. The G mode of graphite comes from the bond stretching of pairs of sp^2 C atoms and it is not dependent on sixfold rings thus occurring at all sp^2 sites including chains. The D peak is a breathing mode of aromatic rings and while the G band does not require sixfold rings, the D band does. This mode is active solely in the presence of disorder and it is forbidden in perfect graphite. The same characteristic bands, but with modified parameters are prominent in the Raman spectra of the carbon structures along the amorphization trajectory despite them not having broad graphitic ordering. The Raman spectrum of free MB presents very well defined sharp peaks that can be attributed to specific vibrations mode of the fluorophore molecule (Figure S1). For the MB solutions exposed at different plasma treatment, the Raman spectra show well defined G and D peaks, distinct to carbon structures. On the other hand the specific peaks of free MB are decreased in terms of intensity or are entirely vanished. This is evidence

Table 2 Raman deconvolution peak characteristics for the structures obtained with Ar and He plasma at 20 minutes and the maximum time treatment

	D peak (cm^{-1})	FWHM _D (cm^{-1})	G peak (cm^{-1})	FWHM _G (cm^{-1})	I _D /I _G
Ar intermediate	1367	198	1583	121	1
Ar final	1370	244	1581	139	1
He intermediate	1361	258	1575	168	1.1
He final	1353	180	1582	125	0.9

of the simultaneous MB degradation and particle synthesis process. The plasma on the one hand breaks the MB molecules while at the same time acts as an active environment in the synthesis of carbon structures. The G peak in the Ar plasma treated samples appears around 1581 cm^{-1} and has slightly increased width value for the structure at the final plasma treatment time.

The D peak of the intermediate sample is located around the same frequency though it is wider than the final sample. The I_D/I_G ratio is maintained throughout the plasma treatment. For the samples treated with the He plasma, the G width value is higher while the peak position is lower for the intermediate time sample.

The D peak moves to a lower frequency and becomes sharper as the time treatment increases. Regarding the I_D/I_G peak ratio, the value changes from 1.1 at the intermediate time to 0.9 at the maximum treatment time.

One first clue regarding the structure of the particles is given by the I_D/I_G peak ratio. The ratios for the samples have non-zero values close to 1 which is consistent with stages 1 and 2 of the amorphization trajectory. The stage 1 structures should present well defined second order peaks which are absent in this case. However, the spectra do present small broad features in the 2400-3100 cm^{-1} region, a feature of stage 2. Stage 2 represents the transition from nanocrystalline graphite to low sp^3 amorphous C. As the carbon structure changes towards a higher amorphous state, the G peak position shifts to lower frequencies and simultaneously the I_D/I_G peak ratio decreases.

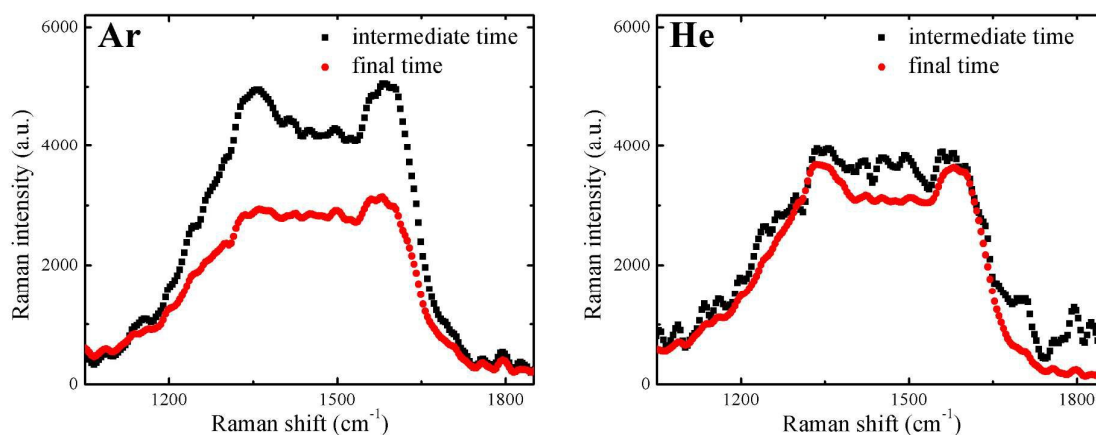


Figure 7 - Raman spectra of the particles obtained with Ar plasma (left) and He plasma (right) at 20 minutes and the maximum time treatment.

During this stage, defects are further induced in the structure, the sp^3 C content increases and the rings get more distorted even to the level of opening up. This means that the band ratio decrease is due to the D peak rather than the G peak whose intensity is related to the relative motion of the sp^2 carbon atoms, unmodified by the rings distortion.

Unlike the case of graphite, when the increase of D peak intensity indicates disordering, for stage 2 carbons the D peak intensity increase is a sign of ordering as the peak relates directly to the number of ordered rings in this stage^{14,22}.

For the particles obtained with the Ar plasma, the Raman spectra reveal one important piece of information. The G peak remains approximately at the position and the I_D/I_G peak ratio does not change significantly as the plasma exposure time increases. This might seem to indicate that there is a saturation-like regime in the particle synthesis during which the plasma does not aid in the progress of the synthesis. However, the D peaks broadens with the increase of plasma exposure time a clear indicator of rings with higher order than six and the G peak broadens as well. An important conclusion arises: the plasma has a destructive effect on the particles as well. This result is consistent with the TEM images which indicate the plasma degradation effect on the particles. As the plasma acts on the particles smaller ordered domains are produced and the D peak increases slightly in intensity. The distortion and structure modification could be induced indirectly by the plasma through the interaction with the oxidative species or directly via energetic electron bombardment and ion collisions.

The evolution of the Raman spectra of the carbon particles obtained with the He plasma points towards an ordering of the structure as the plasma exposure time increases. The G peak does shifts to higher frequencies while the solution is further exposed to He plasma, even if the I_D/I_G peak ratio does not modify sufficiently to be taken into account (the difference might come from spectra processing errors). The G width, which decreases during plasma treatment, is evidence for the ordering of the structure, as well. The D peak reveals additional structural information since ring orders other than six tend to decrease the D peak height and increase its width. At the intermediate time, the D peak width of the particles is larger than for the particles at the end of the treatment. Thus, as the plasma exposure proceeds fewer higher ring orders are found in the structure. The carbon particle synthesis process is consequently a progressive one, starting from MB degradation products that built up together to form a more ordered/less amorphous structure as the plasma exposure advances.

From the Raman spectra specifically, the destructive effect is visible only for the Ar plasma which was previously characterized as more aggressive in terms of the dye degradation capacity due to the active species which are more energetic and in greater quantity than for the He plasma. At the chosen intermediate time, the Ar plasma had degraded almost the entire MB molecules while the He plasma did not. Presumably, in the case of the He plasma the destructive effect of the plasma is disguised by the constructive one while for the Ar plasma the constructive effect is greatly reduced in

the last minutes of the treatment due to the lack of MB molecules.

XPS analysis

XPS is the most suitable technique in analyzing the surface of materials and particles which could provide insight into the surface interaction of the material with other bodies. In our previous work we performed XPS measurements on the particles obtained with the Ar plasma after complete MB degradation. We complete our findings with the analysis of the particles synthesized aided by the He plasma and compare the two cases. A comprehensive description of the high resolution peak deconvolution is given in electronic supplementary information. The elemental concentrations at the surface before and after plasma treatment are shown in table 3. Carbon is the prevalent surface component in the control sample (before treatment) but also for the particles obtained with Ar and He plasma. In the case of the He plasma the ratio C:O drops from 8.3 before treatment to 2.4 after treatment indicating that oxygen is involved in the new bonds within the products formed during the plasma treatment. For the Ar plasma the C:O ratio at the surface is 3.6 less than before treatment but higher than for the case of He suggesting that at the surface of the particles there are more oxygen moieties for the He plasma. At a first glance, this seems to contradict the fact there is a greater amount of oxidative species in the Ar plasma, still the higher He plasma treatment time should be taken into account. This allows the He plasma to interact with the particles for a longer period of time and further increase the oxygen content at the surface. Regarding the C1s spectrum (figure 8), after the He plasma treatment the main contributions assigned to C-C/C=C and C-N/C=N/C-S become broader around 2.5 eV (Table S1). The broadening indicates that changes occurred in the MB molecule during plasma exposure nevertheless they cannot be distinguished mostly due to the overlap of the C-S, C=N, C-N which appear in proximity to each other²³⁻²⁵. A new peak appears at 288.1 eV probably because of the formation of N-C=O, amide type bonds at the surface²⁶. Similarly to the He plasma treatment for the Ar plasma, a new peak is formed at higher binding energies probably because of the formation of N-C=O at the surface²⁶.

In both cases, the N-C=O functional group has an approximately 9 % contribution to the overall peak. It is important to mention that C-C/C=C peak has a more significant contribution in the overall peak for the He plasma than the Ar plasma case. This is in agreement with the Raman findings that the He plasma particles have a higher ordering of the carbon structure at the end of treatment while the Ar plasma particles

Table 3 - Elemental concentrations at the surface for MB solutions before and after plasma treatment

	C 1s	O 1s	N 1s	S 2p
Before treatment ¹⁰	77.6	9.3	9.6	3.5
Ar plasma treatment ¹⁰	72.3	20.2	4.8	2.7
He plasma treatment	58.7	24.3	10.4	6.6

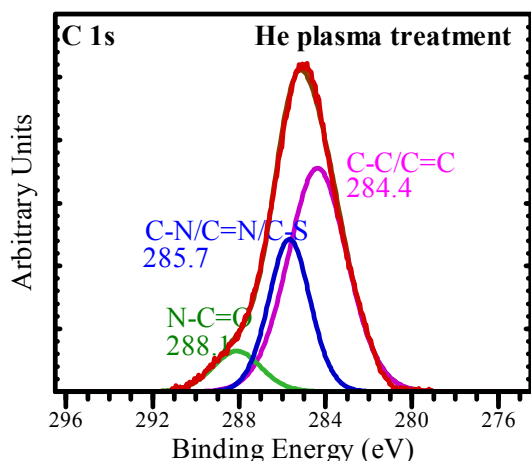


Figure 8 - C1s high resolution spectrum for the structures obtained with He plasma after the maximum time treatment

have an increased amount of defects at the end of treatment. The XPS reveals the possible nature of several of these defects, at least at the surface, such as sites where the C-C/C=C bonds are replaced by C-N/C=N/C-S bonds and lead to higher order rings in the structure. The defects are not present exclusively on the surface of the particles obtained with the Ar plasma, but rather they seem to balance, in terms of relative abundance, the C-C/C=C bonds in the surface structure.

Overall, the oxygen content at the surface is higher for the particles obtained with the He plasma suggesting there are more functional groups with oxygen on their surface compared to the Ar plasma case. One expects for the particles with more oxygen at the surface to have the higher amount of defects which is incongruous with the results. The explanation lies in the analysis of the other peaks. The N 1s and S 2p peak show at the surface of the particles, the presence of higher oxidation state compounds for the particles obtained with the He plasma versus the Ar plasma which is consistent with the higher time treatment for the He plasma. The additional oxygen atoms in the case of the He plasma contribute to the increase of the oxidation state of the functional groups rather than form new ones which might lead to an increased amount of defects. Furthermore, in the O 1s and N 1s peaks (see Table S3, S4), new contributions develop for the samples treated with plasma, contributions supporting the formation of N-C=O functionality assigned to the new peak in C1s.

Carbonaceous structures synthesis mechanism

We propose the following mechanism for the synthesis of carbonaceous structures by plasma in contact with MB solutions schematically represented in figure 9. As the MB molecules are exposed to plasma, generated inside the solution, three main degradation mechanisms occur simultaneously. Oxidative species (e.g hydroxyl), high energy electrons accelerated by the radiofrequency field and plasma gas ions act on the MB molecules which results in the breaking of the bonds forming the molecules. There are three possible

starting degradation routes suggested by the analysis techniques: demethylation at the side N atoms evidenced by the blue-shift of the main absorption band, central ring opening at N or S site consistent with the intensity decrease of main band assigned to a $n \rightarrow \pi^*$ transition and side ring opening at one of the C atoms also correlated to the disruption of the π -conjugated system. Presumably, the active species in the plasma continue to interact with the molecules to form numerous fragments as more bonds are broken. Part of these fragments undergo complete degradation while concomitantly, other fragments attach to one another to form new structures. To satisfy all the bonds of the carbon atoms in the resulted fragments, new bonds with the oxidative species are formed as suggested by XPS which shows an increase of oxygen content at the surface for the carbonaceous structures. The plasma has a double role. On the one hand, it acts as an active environment in this process, due to its reducing capabilities which aid in the formation of new carbonaceous structures. On the other hand, it has a degradation effect on the newly formed structures visible in the Raman spectra. Depending on the type of gas used to generate the plasma, Ar or He, the carbon based structures have at the end of synthesis a different degree of disorder and amorphization and surface functional groups (see Table S2, S4).

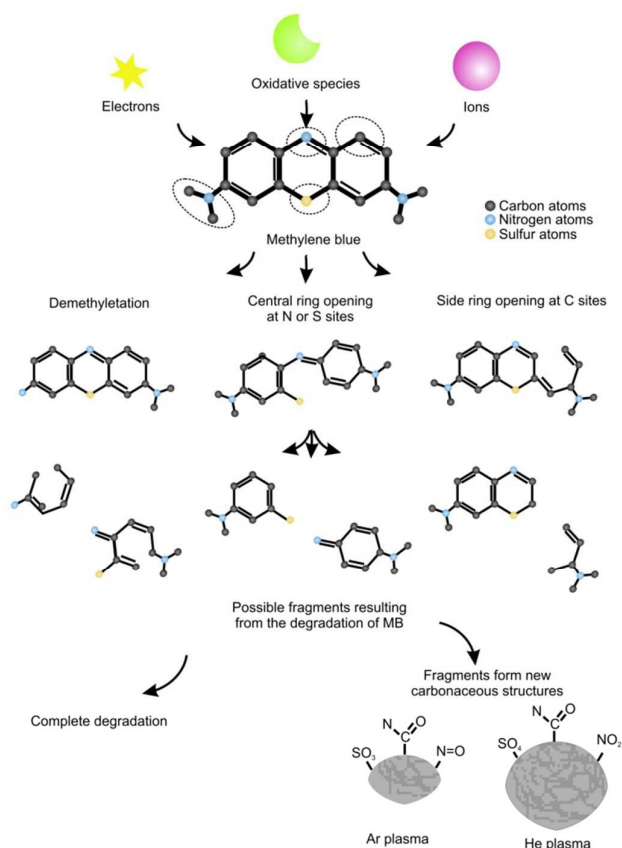


Figure 9 – Proposed carbonaceous structures mechanism by plasma inside MB solutions

Bacterial growth inhibition assay

We chose to do the antibacterial assay with the structures obtained after the maximum plasma treatment, due to the antiseptic nature of MB which would interfere in the results. The bacterial growth curves are presented in figure 10. The particles obtained with the two types of plasmas have remarkably different effects on *E.coli* bacteria. One inhibits the growth as the particle concentration increases while the other favors it. The inhibition capacity of the He plasma particles seems to depend only slightly on the particle concentration the inhibition capacity having values in the 19-26 % range for all the concentrations used. For the other particles, values, ranging between 15-54% for favoring the bacterial growth, were recorded.

In general terms, the antimicrobial activity of the nanoparticles depend on their composition, surface structure, intrinsic properties, and the type of microorganism they act on³. The interaction of bacteria with nanoparticles results in formation of cavities in the bacterial cell wall and the accumulation of nanoparticles in the membrane due to their high affinity to interact with membrane components, mainly phospholipids. The deposition of nanoparticles leads to a significant increase in membrane permeability and loss of integrity, resulting in the cell death^{27,28}.

For carbon-based nanomaterials, recent studies show that the direct physical interaction with bacteria and not oxidative stress, is the main antimicrobial mechanism³. The size was reported to be an important parameter. As the size decreases down to nanoscale the surface area increases significantly and so does the area of interaction between the cells and the nanoparticles³. Perreault *et al* show that the size might have opposite antibacterial effects when doing the assay in suspension or solid substrates²⁹. Graphene oxide with smaller lateral size sheets has an increased antimicrobial effect on *E.coli* when deposited on substrates compared to bigger sheets whereas the bigger sheets are more efficient when in suspension. This was associated with the capacity of larger sheets to isolate the cells from their environment as they completely fold and cover the cells in suspension.

The differences occurring between the two types of carbon particles in this work might be explained by their different sizes. The evaluation was made in suspension therefore it is not surprising that the particles larger in size inhibit the growth of the bacteria. The inhibition capacity could also be explained by the surface oxidation level of the structures obtained with He plasma. In a study made on graphene oxide and reduced graphene oxide, better antibacterial activity was recorded for graphene oxide, the structure with a higher level of oxidation, despite the fact the reduced form had higher lateral dimensions³⁰. As measured by XPS, the structures obtained with He plasma do present at their surface functional groups with a higher oxidation number than the structures obtained with Ar plasma, which might enhance their bacterial growth inhibition capacity. The mechanism for bacterial inactivation is not clear however. We presume that as the cell directly interacts with the particles both physically and chemically via the functional groups, the bigger structures encase the entire

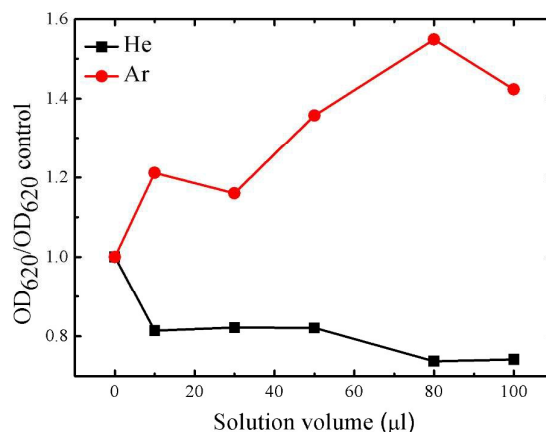


Figure 10 - *E.coli* bacterial growth curves for the structures obtained with He and Ar plasma after complete MB degradation

cell and it isolates it from the resources necessary to proliferate. As for the smaller structures, even if the functional groups at the surface might promote bacterial interaction, there is only a low probability for smaller particles to cover the entire bacterial cell so that it would isolate it from the environment. They act more as anchors for the bacteria as they still have access to nutrients and they continue to grow.

Conclusions

Gas bubbled plasmas operating at pressures slightly higher than the atmospheric pressure inside liquid are used to synthesize carbon particles from MB solutions. Simultaneously, plasma degrades the dye and provides the building blocks for the particles. We show that the working gas He and Ar respectively, have a different degradation effect on the solution and also a direct influence on the structure and morphology of the particles. The Ar plasma was termed as more aggressive as the active species are more energetic and in a greater amount than the He plasma. The TEM analysis showed that the structures obtained with the He plasma are larger compared to the case of the Ar plasma and revealed that the plasma has a destructive effect on the structures as well.

Raman spectroscopy revealed that the obtained structures are between nanocrystalline graphite and low sp³ amorphous carbon. In the case of the He plasma, the structure becomes progressively more ordered as the degradation products build-up while the Ar plasma induces more defects in the structure as the plasma exposure proceeds. The plasma degradation effect on the particles was not excluded in the case of the He plasma. The XPS analysis confirmed the higher ordering level of the structures obtained with the He plasma and revealed the presence at the surface of functional groups such as amide and others with a higher oxidation degree for the case of He plasma.

The *E.coli* bacterial growth inhibition capacity of the obtained structures was evaluated. A growth inhibition effect was observed for the case of He plasma carbon structures while an

opposite effect was recorded for the case of Ar plasma. The different effects were associated with the larger size of the He plasma carbon structures. Further research is required to elucidate the bacterial inhibition mechanism and the factors that govern the bacterial growth promotion for the case of the Ar plasma.

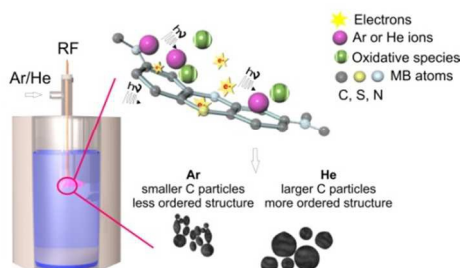
Acknowledgements

Author Diana Zaharie-Butucel gratefully acknowledges the financial support of the Sectoral Operational Programme for Human Resources Development 2007-2013, co-financed by the European Social Fund, under the project POSDRU/187/1.5/S/155383- "Quality, excellence, transnational mobility in doctoral research".

Authors want to thank as well dr. Teodora Radu, dr. Adriana Vulpoi and assist. prof. dr. Nicolae Leopold for their help in performing several of the measurements. Authors are especially grateful to Iulia Elena Vlad, for her support in the synthesis procedure under deadline pressure.

References

- C. Cheng, A. E. Porter, K. Muller, K. Koziol, J. N. Skepper, P. Midgley and M. Welland, *J. Phys. Conf. Ser.*, 2009, **151**, 012030.
- N. Lewinski, V. Colvin and R. Drezek, *Small*, 2008, **4**, 26–49.
- S. M. Dizaj, A. Mennati, S. Jafari, K. Khezri and K. Adibkia, *Adv. Pharm. Bull.*, 2015, **5**, 19-23.
- M. M. A. Rafique and J. Iqbal, *J. Encapsulation Adsorpt. Sci.*, 2011, **01**, 29–34.
- A. P. Demchenko and M. O. Dekaliuk, *Methods Appl. Fluoresc.*, 2013, **1**, 042001.
- P. Bruggeman and C. Leys, *J. Phys. Appl. Phys.*, 2009, **42**, 053001.
- I. E. Vlad, O. T. Marisca, A. Vulpoi, S. Simon, N. Leopold and S. D. Anghel, *J. Nanoparticle Res.*, 2014, **16**.
- M. A. Bratescu, S.-P. Cho, O. Takai and N. Saito, *J. Phys. Chem. C*, 2011, **115**, 24569–24576.
- J. Senthilnathan, Y.-F. Liu, K. S. Rao and M. Yoshimura, *Sci. Rep.*, 2014, **4**.
- S. D. Anghel, D. Zaharie-Butucel and I. E. Vlad, *J. Electrostat.*, 2015, **75**, 63–71.
- D. Zaharie-Butucel, S. D. Anghel, *Rom. J. Physics*, 2014, **59**, 757–766.
- H. Luque and D. R. Crosley, *Stanford Research Institute (SRI) International Report M MP 99-009*, 1999.
- S. Hofmann, A. F. H. van Gessel, T. Verreycken and P. Bruggeman, *Plasma Sources Sci. Technol.*, 2011, **20**, 065010.
- A. C. Ferrari and J. Robertson, *Phys. Rev. B*, 2000, **61**, 14095–14107.
- S. D. Anghel, A. Simon, A. I. Radu and I. J. Hidi, *Nucl. Instrum. Methods Phys. Res. Sect. B Beam Interact. Mater. At.*, 2009, **267**, 430–433.
- N. K. Bibinov, A. A. Fateev and K. Wiesemann, *J. Phys. Appl. Phys.*, 2001, **34**, 1819–1826.
- P. Bruggeman and D. C. Schram, *Plasma Sources Sci. Technol.*, 2010, **19**, 045025.
- K. Murugan, T. N. Rao, A. S. Gandhi and B. S. Murty, *Catal. Commun.*, 2010, **11**, 518–521.
- T. Zhang, T. Oyama, A. Aoshima, H. Hidaka, J. Zhao and N. Serpone, *J. Photochem. Photobiol. Chem.*, 2001, **140**, 163–172.
- S. Ikoma, K. Satoh and H. Itoh, *Electr. Eng. Jpn.*, 2012, **179**, 1–9.
- M. Magureanu, N. B. Mandache and V. I. Parvulescu, *Plasma Chem. Plasma Process.*, 2007, **27**, 589–598.
- L. G. Cançado, A. Jorio, E. H. M. Ferreira, F. Stavale, C. A. Achete, R. B. Capaz, M. V. O. Moutinho, A. Lombardo, T. S. Kulmala and A. C. Ferrari, *Nano Lett.*, 2011, **11**, 3190–3196.
- A. Dementjev, A. de Graaf, M. C. van de Sanden, K. Maslakov, A. Naumkin and A. Serov, *Diam. Relat. Mater.*, 2000, **9**, 1904–1907.
- D. R. Dreyer, S. Park, C. W. Bielawski and R. S. Ruoff, *Chem Soc Rev*, 2010, **39**, 228–240.
- A. Vesel and M. Mozetic, *J. Phys. Conf. Ser.*, 2009, **162**, 012015.
- R. A. Rincón, K. Artyushkova, M. Mojica, M. N. Germain, S. D. Minter and P. Atanassov, *Electroanalysis*, 2010, **22**, 799–806.
- I. Sondi and B. Salopek-Sondi, *J. Colloid Interface Sci.*, 2004, **275**, 177–182.
- J. Vidic, S. Stankic, F. Haque, D. Ciric, R. Le Goffic, A. Vidy, J. Jupille and B. Delmas, *J. Nanoparticle Res.*, 2013, **15**.
- F. Perreault, A. F. de Faria, S. Nejati and M. Elimelech, *ACS Nano*, 2015, 150625122551009.
- S. Liu, T. H. Zeng, M. Hofmann, E. Burcombe, J. Wei, R. Jiang, J. Kong and Y. Chen, *ACS Nano*, 2011, **5**, 6971–6980.



A straightforward carbonaceous structures synthesis from methylene blue aided by Ar / He plasmas with different ordering and *E.coli* inhibition effects.